Engineering Failure Analysis 34 (2013) 93–101

Contents lists available at ScienceDirect

Engineering Failure Analysis

journal homepage: www.elsevier.com/locate/engfailanal

Dynamic dragline modeling for operation performance simulation and fatigue life prediction

Ying Li [a,*], Wenyuan Liu [b]

[a] Bucyrus International, Inc., South Milwaukee, WI 53154, USA
[b] Washington University in St. Louis, MO 63103, USA

ARTICLE INFO

Article history:
Received 1 May 2012
Accepted 17 July 2013
Available online 31 July 2013

Keywords:
Dragline
Dynamic model
Virtual prototype
Co-simulation
Fatigue life

ABSTRACT

In this study, the three-dimensional (3D) dynamic dragline models are developed for investigating the dynamic dragline performance and front-end structural strength. A virtual prototype of the dragline is created by the dynamic integration of the mechanical and electrical system models using Newton–Euler equations. The mechanical model is modeled as a rigid multi-body system to catch the major kinematics and dynamics behavior of the whole dragline. The electrical model is employed to represent the motors and controls. The dragline front-end is modeled as a flexible multi-body system for the structural strength evaluation using Lagrange equations and finite element analysis (FEA) method. A co-operative simulation (co-simulation) is carried out with the dragline motion, electrical motor/control and the structural flexibility models. The major motions, the machine behavior, the machine operation loads, and structural member stresses are recovered from the simulation. The results of stress-time history are used for structural fatigue life evaluation by Palmgren–Miner's rule. The results show the boom structural members have lower fatigue lives than tri-structure structural members. The study is significant to provide a solid foundation for further study of failure life analysis of the whole dragline components.

1. Introduction

A dragline is a large rotating multi-body system to remove overburden in surface mining environment. The repeated dynamic, instantaneous loading accumulates over the dragline service life, and it may induce front-end damage. Fatigue failure in components causes unplanned downtimes, reduced efficiency and high production costs. The primary objective of this study is to examine dragline front-end life towards efficient operation. The structural loading on dragline front-end depends mainly on the rated suspended load, and the accelerations created by hoist and swing motors. Other factors such as the digging pattern, operator characteristics and electrical motor control systems also influence the loading on front-end [4]. In order to calculate the overall stress loading of front-end, it is necessary to build the dragline virtual prototype just as to build a physical prototype. For this purpose, 3D dynamics of the dragline must be modeled and analyzed.

Conventional design process uses a laboratory test to simulate the dragline front-end to detect the cracking for the reduction of component fatigue failure. This process is very costly and time-consuming for achieving statistically significant basis for evaluation and subsequent decisions. Previous researchers have developed a dynamic model in dragline operation and studied the component fatigue failure by the field-testing data or FEA [8,4,2]. Recently, virtual prototype simulators have been used to simulate surface mining equipment [9]. Modern design processes in virtual simulation environments enable the testing of machine performance and component fatigue failure prior to final design and field-testing. The major failure

* Corresponding author.
E-mail address: liyinglzh@yahoo.com (Y. Li).

1350-6307/$ - see front matter © 2013 Elsevier Ltd. All rights reserved.
http://dx.doi.org/10.1016/j.engfailanal.2013.07.020

modes of dragline are crack and fracture caused by fatigue stress in dragline excavation [8]. FEA can be used for computing stresses in dragline components. Input into such a programme must include a complete description of the forces acting on the components via dynamic modeling.

Dragline is a multi-degree of freedom and non-linear multi-body dynamic system. Thus, rigid and flexible multi-body dynamics theory is used to develop its dynamic models and component stress loading using Newton–Euler and Lagrange equations, and FEA method [11]. The ADAMS, MATLAB/Simulink and ANSYS software [10,1] allow to build the mechanical system, the electrical motor control, and the structural flexibility models, respectively. These software packages contain computationally efficient numerical simulation routines to solve the kinematics, dynamics and stress equations. A co-simulation allows to couple these models together to produce a full virtual prototype for executing realistic system dynamics and structural dynamics simulation of complex dragline systems [12]. The fatigue lives for the structure members can be examined using Palmgren–Miner's cumulative damage criterion [6].

2. Structural components of the dragline front-end

Fig. 1 illustrates a schematic diagram of walking dragline. The lower body provides a stable base for the dragline. The upper body provides a platform for the hoist-drag-swing machinery, boom and tri-stricture attachment, electronic control cabinets, operator's cab and supporting equipment. The front-end mechanism consists of a large bucket which is suspended from a boom with wire ropes. The bucket is maneuvered by hoist and drag ropes, powered by electric motors. The work cycle of the dragline consists of three distinct phases, including digging, swinging, and swinging back. In a digging phase, the bucket is positioned above the material to be excavated. Then, the bucket is lowered and the drag rope is drawn so that the bucket is dragged along the surface of the material. The bucket is lifted by using the hoist rope. A swing operation is performed to move the bucket to the place where the material is to be dumped. The drag rope is released causing the bucket to tilt and empty by the dump operation. Finally, the bucket is swung back to repeat the cycle.

3. Virtual prototype modeling of the dragline

Fig. 2 depicts a 3D virtual prototype of the dragline created by the dynamic coupling the mechanical and electrical system models. The mechanical model is modeled as a rigid multi-body system in the ADAMS environment to catch the major dynamic behavior of the whole dragline. Simulink is employed to represent the motors and controls. ADAMS/Controls are used to link the two models to co-simulate the mining dragline. The modeling steps are indicated below.

The first step involves the creation of 3D geometrical models of key components as shown in Fig. 2. The model contains lower body, revolving frame, machinery house, operator's cab, tri-stricture, boom, hoist and drag ropes, and bucket. Inertias, weights and other physical characters, which influence the behavior of the dragline, are included in the model. The

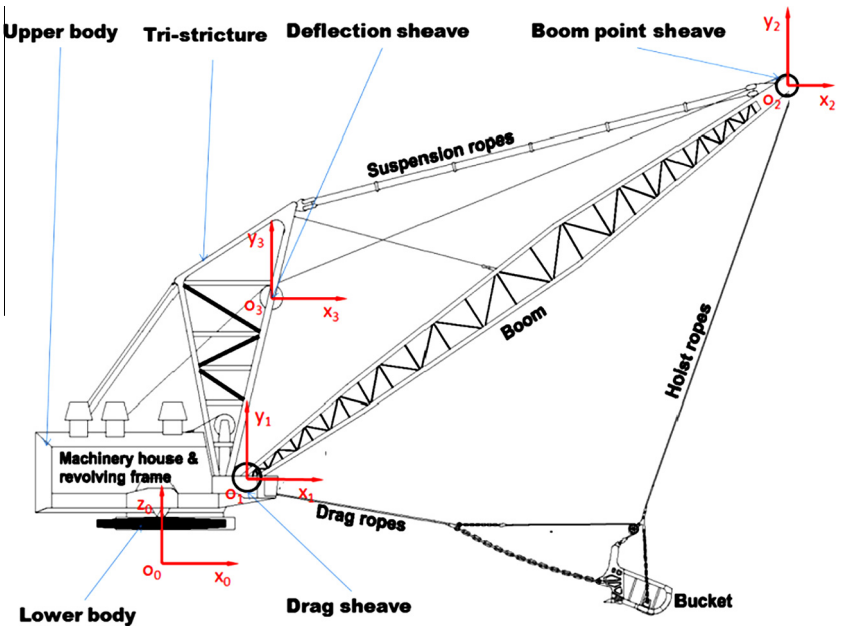

Fig. 1. Dragline front-end schematic diagram (http://www.bucyrus.com).

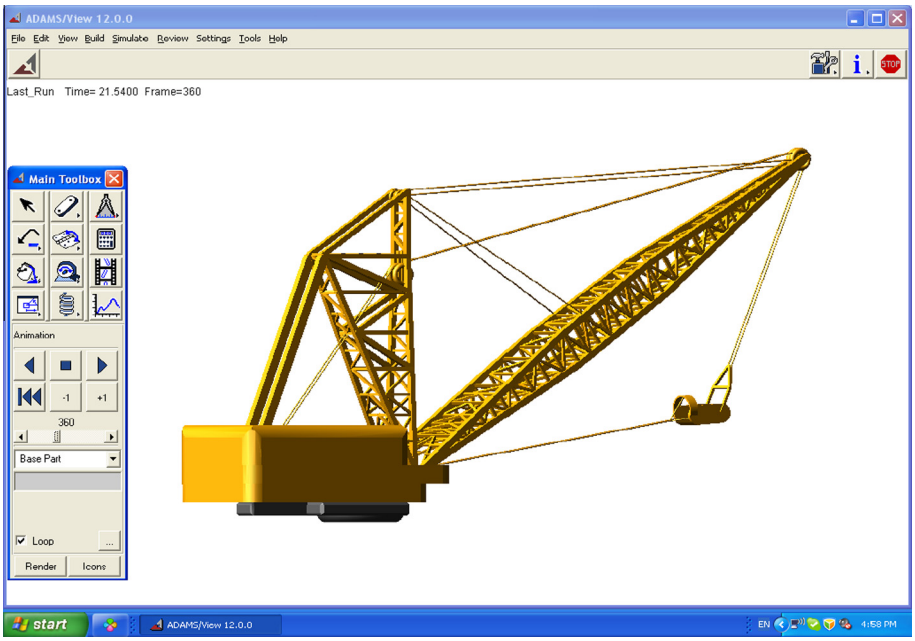

Fig. 2. Dragline virtual prototype model.

components are regarded as an assemblage of multi-rigid-bodies, connected by joints, to form a kinematics chain with one link fixed that transforms the generated motions.

The second step defines the boundaries of the components with joints and the appropriate algebraic variables, which represent the component movements based on the rigid multi-body system equations [11]. The appropriate dynamic model of the system is given by Newton–Euler Eq. (1).

$$\tau = M(\Theta)\ddot{\Theta} + V(\Theta, \dot{\Theta}) + G(\Theta) + F(\Theta, \dot{\Theta}) \tag{1}$$

τ is the vector of joint torques, $M(\Theta)$ is the $n \times n$ inertia matrix of the system, $V(\Theta, \dot{\Theta})$ is the $n \times 1$ vector of centrifugal and Coriolis terms, $G(\Theta)$ is the $n \times 1$ vector of gravity terms, and $F(\Theta, \dot{\Theta})$ is the $n \times 1$ vector of friction.

The third step introduces force elements to the model. The bucket resistances from ground and payload are adopted for the model. The model is driven and controlled by electrical motors with the motor characteristic built in the Simulink power train models as given in Fig. 3. It includes the speed-torque, ramp, and any associated control settings. The electrical motors generate torques for the swing, hoist and drag ropes motion. The torques are determined by the velocity and displacement of the swing, hoist and drag ropes which are calculated from the mechanical dynamics of the dragline. The dynamics of the system is highly nonlinear. The control torque at the driving joints is developed using multi-input and multi-output control system [3] as expressed by the following equation:

$$\tau = \alpha\tau' + \beta \tag{2}$$

where

$$\alpha = M(\Theta) \tag{3}$$

$$\beta = V(\Theta, \dot{\Theta}) + G(\Theta) + F(\Theta, \dot{\Theta}) \tag{4}$$

with the servo law

$$\tau' = \ddot{\Theta}_d + K_v\dot{E} + K_pE \tag{5}$$

where

$$E = \Theta_d - \Theta \tag{6}$$

$$\dot{E} = \dot{\Theta}_d - \dot{\Theta} \tag{7}$$

K_v and K_P are $n \times n$ matrices of constant gains, E and $\dot{E}$ are $n \times 1$ vectors of errors in position and velocity, respectively, and Θ_d is the victor of the desired joint angular displacement. This means that the motions or torques applied to the swing, hoist and drag ropes are introduced during operation. Using the ADAMS software, differential-algebraic equation systems are

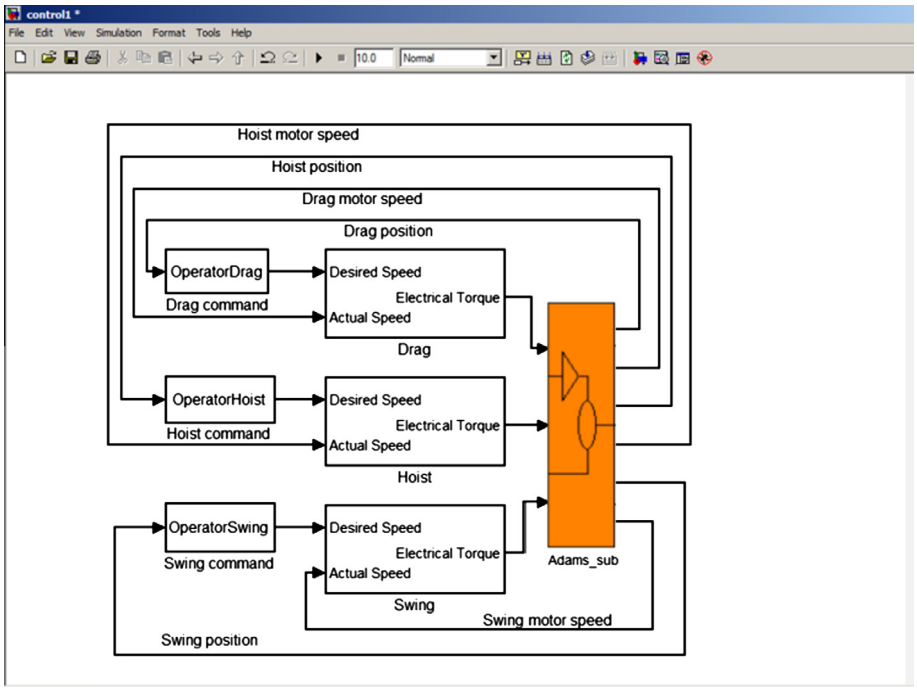

Fig. 3. Dragline control model.

derived and integrated in time to perform the model dynamic simulation. The movements of the model depend on interactive elements like massless joints, which constrain the relative movements of the dragline components.

4. Flexible multi-body modeling of the dragline front-end

Fig. 4 indicates the dragline front-end flexible FE model created in ANSYS environment with the global coordinate attached to the ground at the revolving frame pintle. The front-end parts are created as flexible bodies. They are the beam elements for the boom and tri-structure, link elements for the cables, shell elements for the rigid revolving frame and mass

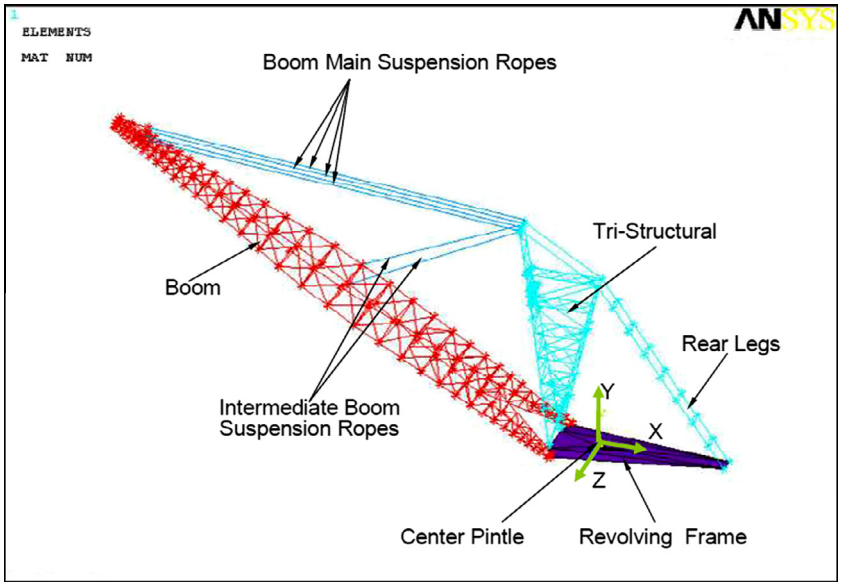

Fig. 4. Dragline front-end FEA model.

elements to add miscellaneous weights to the nodes. The hoist and drag ropes, and bucket are not included in the model. The material properties are chosen for the components with the elasticity modulus of 206.7 GPa, Poisson's ratio of 0.3, and density of 7820 kg/m^3. The kinematic constraints or forces are applied to these boundary nodes served as interface to connect two parts and the remaining nodes are referred to as interior nodes. The model is restrained in the x, y and z axial directions, and x and z rotation directions at the center pintle. The major motion loads going into the front-end includes the digging, hoisting, swinging, dumping, and swinging back. The main load components going into the structure include loads at the boom point, loads in the hoist rope acting onto the deflection sheave, loads due to swing acceleration that causes structural inertia loads, and side loads at the boom point from the hoist rope. The Lagrange motion equation for the flexible body [7] is derived from the following equation:

$$M\ddot{\xi} + \dot{M}\dot{\xi} - \frac{1}{2}\left[\frac{\partial M}{\partial \xi}\dot{\xi}\right]^T \dot{\xi} + K\xi + \frac{\partial V_g}{\partial \xi} + D\dot{\xi} + \Psi_\xi^T \lambda = Q \tag{8}$$

where ξ are the generalized coordinates, M is the generalized mass matrix, K is the generalized stiffness matrix, V_g is the gravitational energy, D is the damping, Ψ is the kinematic constraint equations applied to the flexible body, λ is the Lagrange multipliers and Q is the generalized applied forces.

5. Dynamic simulation of the dragline

A co-simulation is carried out with the dragline motion from the ADAMS simulation, the electrical motor/control from the Simulink model, and the structural flexibility from the ANSYS model. The major motions, the machine behavior, the machine operation loads, and structural member stresses are recovered from the simulation. The results are used for the structural endurance evaluation.

5.1. Virtual prototype simulation results

The motion of the dragline mechanism is visualized by plotting successive linkage positions on graphic displays in the ADAMS environment. The motion presented in this example includes the digging, swinging, and swinging back. The dragline dynamic behavior and operation loads are recovered from the simulation.

Fig. 1 illustrates that four coordinate systems are chosen in the model. o_0 ($x_0y_0z_0$) coordinate system is attached at point o_0 of the lower. o_1 ($x_1y_1z_1$) coordinate system is attached to the upper at the joint point o_1. o_2 ($x_2y_2z_2$) coordinate system is attached to the boom at the joint point o_2. o_3 ($x_3y_3z_3$) coordinate system is attached to the tri-stricture at the point o_3.

The simulation results are obtained within the working time of 60 s (10 s for digging, 27 s for swinging and 23 s for swinging back). Fig. 5 shows the respective loading on the boom point sheave, drag sheave, and upper swing in appropriate coordinate systems. The angular displacement of the boom point sheave variation with time relative to the o_2 ($x_2y_2z_2$) coordinate system (see Fig. 1) is given in Fig. 5a. The angular displacement of the drag sheave variation with time relative to the o_1 ($x_1y_1z_1$) coordinate system (see Fig. 1) is given in Fig. 5a. The swing upper motion parameters relative to the o_0 ($x_0y_0z_0$) coordinate system (see Fig. 1) is indicated in Fig. 5b.

Fig. 6 gives the superimposed display of the deployment history of the dragline virtual prototype. The appearance of continuous motions of the virtual prototype during the digging, swinging and swinging back phases are shown by plotting successive positions on three graphic displays as illustrated in Fig. 6a–c during 60 s respectively. Examination of the front-end mechanisms shows no interference between two motion components during the operation.

Fig. 7 shows that the output motion results of the bucket during the operating time 60 s. It demonstrates the spatial trajectories with a typical loading cycle comprised of dropping the bucket in the pit, filling the bucket by dragging it towards the machine, lifting the bucket off the ground, swinging the front-end while raising the bucket further, decelerating the

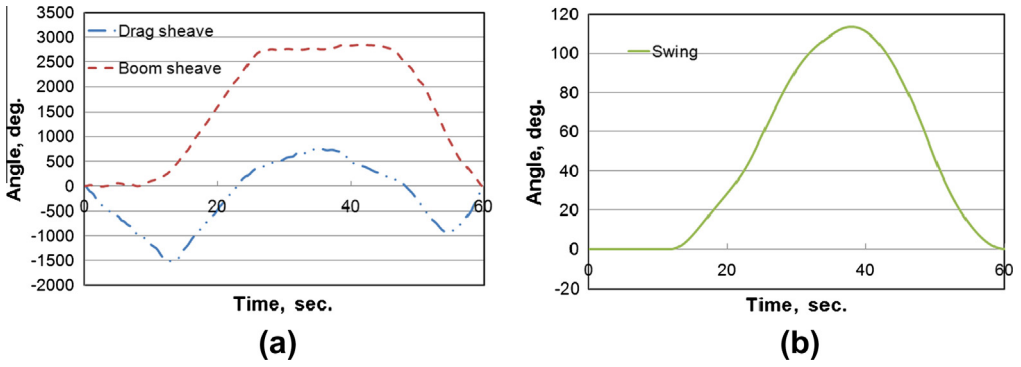

Fig. 5. Angular displacements applied to the dragline system with time: (a) boom sheave and drag sheave, and (b) swing.

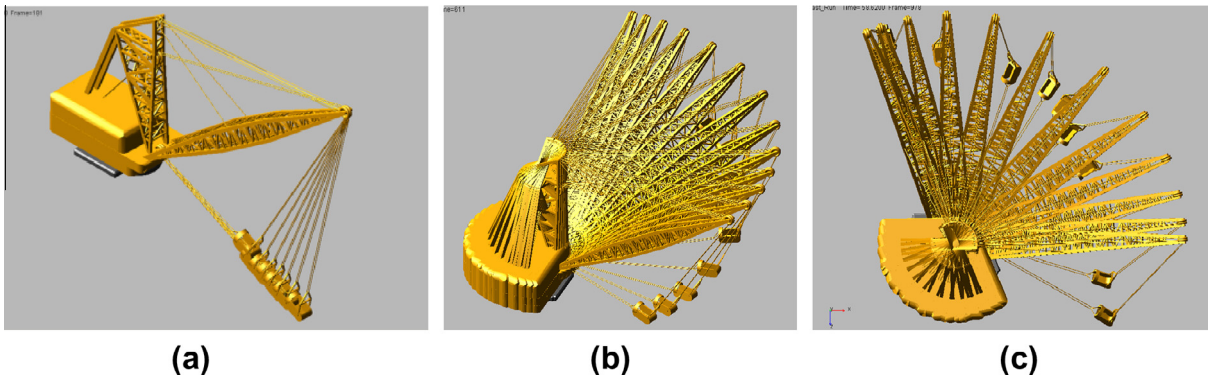

Fig. 6. Superimposed display of the deployment for the dragline in three phases: (a) digging phase from time 0–10 s, (b) swinging phase from time 10–37 s, and (c) swinging back phase from time 37–60 s.

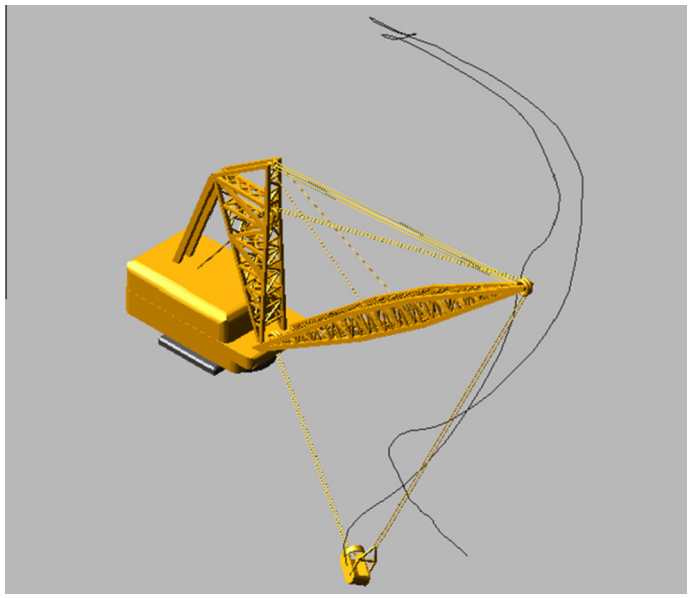

Fig. 7. Bucket spatial trajectory with the operating time 60 s.

swing of the front-end, dropping the bucket load, swinging the front-end in the reverse direction, and returning the bucket to the pit.

5.2. Structure dynamics simulation results

The dynamic loads recovered from the virtual prototype simulation are imported into the front-end FEA model for the structural strength evaluation. Fig. 8a and b indicates the respective loads at the boom point with time of 60 s in the x, y and z directions in the o_2 ($x_2y_2z_2$) coordinate system (see Fig. 1). Fig. 9 displays the respective loads at the deflection sheave with time in the x and y directions in the o_3 ($x_3y_3z_3$) coordinate system (see Fig. 1). The swing angular displacement with time in the z direction is given in Fig. 5b. The transient dynamic analysis is performed for one cycle of 60 s. The time-history axial stress for each structural member is calculated. The tri-structure stress traces for 6 hot spot stress structural members (see Fig. 10a) are pull out as shown in Fig. 11. The boom stress traces for 6 hot spot stress structural members (see Fig. 10b) are given in Fig. 12. The results show that the stress range is variable amplitude. There are compressive stresses in the tri-structure structural members. There are both tensile and compressive stresses in the boom structural members. The boom structural members tend to see a higher stress range. The recovered structural member stresses are processed with Rainflow [5] for cycle-counting the stress range of variable amplitude. For getting variable amplitude fatigue, a variable amplitude stress spectrum is replaced by an equivalent constant amplitude stress range using Palmgren–Miner's cumulative damage criterion [6] by the following equation:

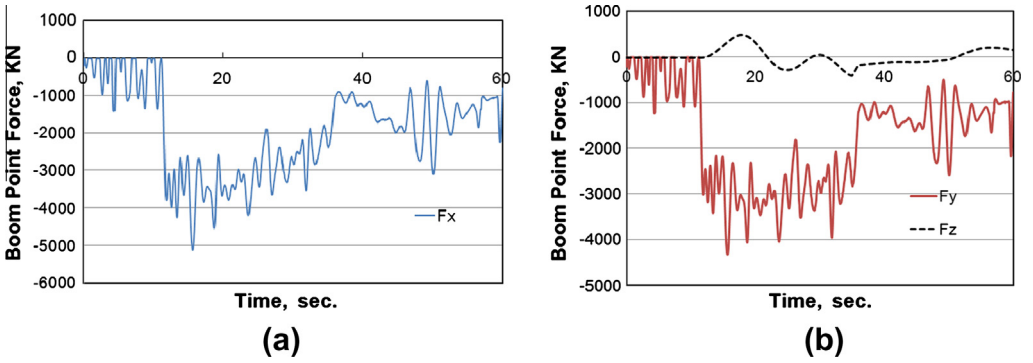

Fig. 8. Dynamic loads at the boom point with time: (a) load in the *x* direction, and (b) loads in the *y* direction and *z* direction, respectively.

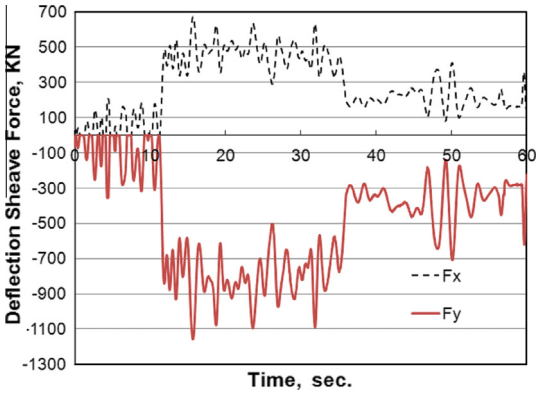

Fig. 9. Dynamic loads at the deflection sheave with time in the *x* direction and *y* direction, respectively.

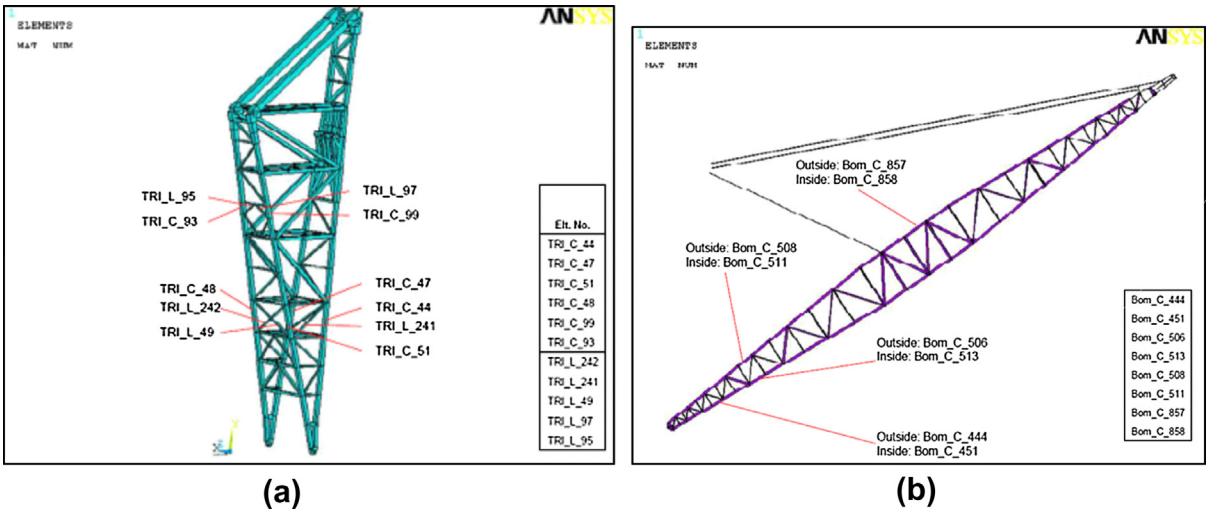

Fig. 10. Element locations: (a) tri-structure and (b) boom.

$$\sigma_v = \left(\sum_{i=1}^{n} (\sigma_i^m N_i)/N_v \right)^{1/m} \tag{9}$$

where *i* is the *i*th stress range in the spectrum, which occurs N_i times, N_v is the equivalent number of stress cycles, and m is the crack growth rate constant.

The dragline operates 1 minute per cycle and 6000 h per year. The life prediction in years is calculated based on the stress range per minute result for each structural member. Table 1 displays the life predictions corresponding to the stress ranges

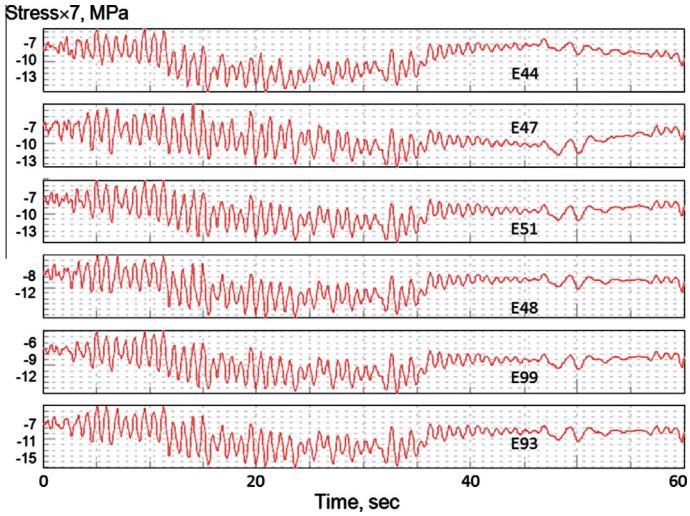

Fig. 11. Tri-structure stress traces for 6 hot spot stress structural members.

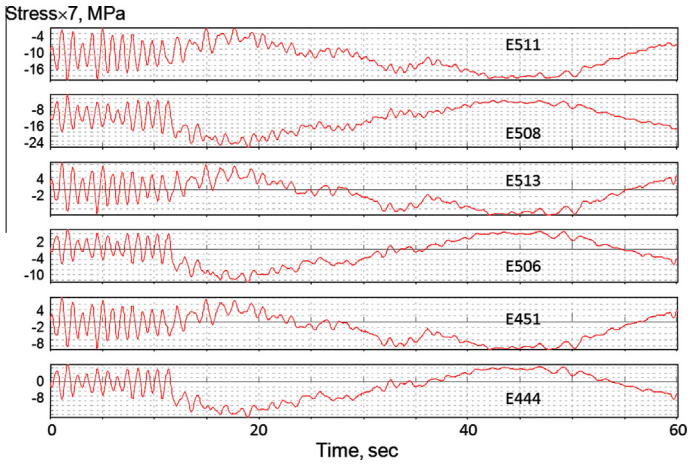

Fig. 12. Boom stress traces for 6 hot spot stress structural members.

Table 1
Dragline front-end life prediction for hot spot stress structural members.

Number element	Stress range (MPa/min)	Life (years)
TRI_C_44	86.66	79.63
TRI_C_47	90.79	66.1
TRI_C_51	98.28	48.14
TRI_C_48	103.6	38.99
TRI_C_99	97.51	49.68
TRI_C_93	99.19	46.4
Bom_C_444	173.6	4.95
Bom_C_451	165.2	5.94
Bom_C_506	158.9	7.03
Bom_C_513	151.9	8.31
Bom_C_508	194.6	3.11
Bom_C_511	193.2	3.19

for the 6 tri-structure and boom hot spot stress structural members, respectively. The results show the boom structural members have lower fatigue lives than tri-structure structural members. The highest fatigue life of 79.63 years with the smallest stress range is at the tri-structure structural member 44. This is because that there is very little cluster cracking in this structural member. The lowest fatigue life of 3.11 years with the largest stress ranges are at the boom structural mem-

ber 508. This is due to the large stress range that drives most of the cracking. The results agree with what are reported in Bucyrus dragline analysis by comparing the dynamic analysis results and the field test data for the boom and tri-structure.

6. Conclusions

Spatial dynamic dragline models are developed by considering the system as a compound of rigid and flexible multi-body dynamics and appropriate dynamics equations are given by Newton–Euler and Lagrangian formulation. A 3D virtual prototype of the dragline is built in ADAMS/Simulink environment. A dragline front-end flexible FEA model is created in ANSYS environment. A co-simulation is given by integrating the mechanical, electrical system and FE models.

From the kinematics, simulation and animation results, it is concluded that the motions for the digging, swinging, dumping, and swinging back can be measured numerically and demonstrated visually. The machine operation loads are measured with selected time steps by simulating reality with this virtual prototype. The superimposed display of the deployment history of the dragline virtual prototype also shows that the dynamic interference among its components can be checked easily. Therefore, this virtual prototype is useful in monitoring motion and identifying possible interference between various components for optimization design or operation of a dragline.

From structure dynamics simulation results, it is concluded that the front-end with all the external loadings and accelerations can be analyzed using FEA model to determine the stresses and stress ranges for all the members of the structural system. The fatigue lives for the structural members are evaluated by Palmgren–Miner's rule. Results show the highest fatigue life of 79.63 years is at the tri-structure structural member 44. The lowest fatigue life of 3.11 years occurs at the boom structural member 508. The simulation results are validated using a test data from Bucyrus, and the validation shows very reliable simulated results.

The simulation presented in this paper forms the basis for complete spatial dynamic modeling and simulation of a dragline. Future research will refine the life prediction method, such as considering the effect of compressive stress, and mean stress. Stress profiles will be calibrated for various sections of the deposit and overburden materials within different locations to serve as standard metrics for operators to attain or to exceed in their performance operations.

Acknowledgements

The authors kindly acknowledge Mr. Shyue-Sheng Chang from Bucyrus International, Inc., USA, for the technical support during the dragline structure dynamics simulation.

References

[1] ANSYS, Inc. Rigid Body Dynamics and the ANSYS-ADAMS Interface. ANSYS Advanced Analysis Techniques Guide, ANSYS; 2011.
[2] Baafi EY, Mirabediny H, Whitchurch K. Computer simulation of complex dragline operations. Int J Surf Min Reclam Environ 1997;11(1):7–13.
[3] Craig JJ. Introduction to robotics: mechanics and control. New York: © Addison-Wesley; 1986.
[4] Dayawansa P, Chitty G, Kerezsi B, Bartosiewicz H, Price JWH. Fracture mechanics of mining dragline booms. Eng Fail Anal 2006;13(4):716–25.
[5] Downing SD, Socie DF. Simple rainflow counting algorithms. Int J Fatigue 1982;4(1):31–40.
[6] Fisher WJ, Kulak GL, Smith IFC. A fatigue primer for structural engineers. National Steel Bridge Alliance Publication; 1998. p. 34–40.
[7] Geradin M, Cardona A. Flexible multibody dynamics: a finite element approach. New York: John Wiley & Sons, LTD.; 2001.
[8] Joshi S, John WH, Price A. Comparative study on application of design codes for prediction of fatigue life of a mining dragline cluster. Eng Fail Anal 2009;16(5):1562–9.
[9] Li Y, Frimpong S. A hybrid virtual prototype for analyzing cable dragline component stress. Int J Adv Manuf Technol 2008;37(5–6):423–30.
[10] MSC Corporation. ADAMS User Manual. © Mechanical Dynamics, USA; 2012.
[11] Synge JL, Griffith BA. Principles of mechanics. New York: McGraw Hill Book Company; 1959.
[12] Zorriassatine F, Wykes C, Parkin R, Gindy N. A survey of virtual prototyping techniques for mechanical product development. In: Proc. Instn. Mech. Engrs. Part B: J. Engineering Manufacture, vol. 217, No. 2; 2003. p. 513–30.